# *In-silico* evidence that increased cortico-thalamic connectivity and superficial pyramidal disinhibition underlie broadband task-related spectral changes induced by ketamine

Alexander D Shaw[1], Suresh D Muthukumaraswamy[2], Neeraj Saxena[1,3], Natalie Adams[4], Rosalyn J Moran[5], Krish D Singh[1]

**Affiliations**

[1]Cardiff University Brain Research Imaging Centre (CUBRIC), Cardiff University, CF24 4HQ, UK

[2]School of Pharmacy, Faculty of Medical and Health Sciences, University of Auckland, Auckland, New Zealand

[3]Department of Anaesthetics, Intensive Care and Pain Medicine, Cwm Taf Morgannwg University Health Board, Llantrisant CF72 8XR, UK

[4]Department of Clinical Neurosciences, University of Cambridge, Cambridge CB2 0SZ, UK

[5]Department of Neuroimaging, Institute of Psychiatry, Psychology & Neuroscience, King's College London, London, SE5 8AF, UK

**Word Counts**

Abstract: 174

Introduction: 336

Methods: 1318

Results: 967

Discussion & Conclusions: 1186

Number of figures: 8

Number of tables: 1

Number of equations: 3

**Declarations of interest:** none

**Keywords:** ketamine, oscillations, neurophysiological modelling, neural mass, MEG, DCM

**Abbreviations**: N-methyl-D-aspartate (NMDA), gamma-aminobuyric acid (GABA), α-amino-3-hydroxy-5-methyl-4-isoxazolepropionic acid (AMPA).

Model population abbreviations:

| **Population name** | **Abbrv.** |
|---|---|
| Superficial layer pyramidal (L2/3) | SP |
| Superficial layer interneuron (L2/3) | SI |
| Spiny Stellate (Layer 4) | SS |
| Deep layer pyramidal (Layer 5) | DP |
| Deep layer interneuron (Layer 5) | DI |
| Thalamic projection pyramidal (Layer 6) | TP |
| Thalamic Reticular | RT |
| Thalamic Relay | RL |

## Abstract

Cortical recordings of task-induced oscillations following subanaesthetic ketamine administration demonstrate alterations in amplitude, including increases at high-frequencies (gamma) and reductions at low frequencies (theta, alpha). To investigate the population-level interactions underlying these changes, we implemented a thalamo-cortical model capable of recapitulating broadband spectral responses. Compared with placebo, ketamine was found to increase the decay rate of NMDA receptor currents, decrease the decay rate of GABA-B receptor currents, but had no effect on AMPA or GABA-A currents. Furthermore, ketamine decreased the inhibitory self-modulation of superficial pyramidal populations, increased the inhibitory self-modulation of inhibitory interneurons and increased the strength of the cortico-thalamic projection from layer 6 into thalamus. *In-silico* rectification of each of these parameters to their placebo state revealed the accompanying spectral changes. Similar broadband effects were demonstrated for the NMDA constant and intrinsic connectivity changes, whereby rectification resulted in normalising the amplitude of alpha (increased) and gamma (decreased). While supporting theories of superficial pyramidal disinhibition following ketamine administration, our results suggest a role for altered cortico-thalamic connectivity relevant to understanding ketamine induced cortical responses and potentially identifies a system-level mechanism contributing to its antidepressant effects.

## Introduction

The spectral composition of magnetoencephalographic (MEG) signals derived from visual cortex reflect a complex system of neuronal interactions, revealed as frequency specific oscillations [1,2] and power law-like phenomena. Individual differences in common metrics, such as the peak frequency and amplitude within specific frequency windows, can predict behaviours[3], disease states[4–9], and are sensitive to experimental manipulations, including pharmacological[10–15].

Oscillations in visual cortex typically demonstrate prominent oscillations in theta / alpha (4 – 7, 8 – 13 Hz), through beta (13 - 30 Hz) up into the gamma (30+ Hz) range[16–22]. Subanaesthetic doses of ketamine, a uncompetitive NMDA receptor antagonist, have been shown to modulate both ends of this spectrum during task, with decreases in the amplitude of lower frequencies[23,24] and increases in the amplitude of higher frequencies [11,23].

While the laminar and network generators of frequency-specific oscillations remain equivocal, prevailing theories propose distinct dominant laminar generators for oscillations of different frequencies. One particular proposal is that high frequencies tend to be formed by current densities in supragranular layers, while lower frequencies appear to predominate in deeper regions of cortex, around layer V/VI [20,25] or in thalamo-cortical loops[26,27]. Under this model, the noted effects of ketamine on both low and high frequency bands suggest altered neuronal functioning across much of the cortical laminae, and possibly in thalamo-cortical connectivity.

Computational modelling is an approach based on the use of basic mathematical descriptions of neuronal units, such as neural mass models, to explore neurophysiological phenomena. Methods such as Dynamic Causal Modelling (DCM) [28–31] provide frameworks for generating typical and atypical empirical features in imaging and electrophysiological time series. In DCM the subsequent fitting (*inverting*) of parameterised mean-field neuronal models to empirical data features, acquired under different pharmacological or task states, permits an *in-silico* assay of usually unobservable neuronal states such as synaptic connectivity between cell populations, or the decay times of specific receptor types. This approach has received construct and face validations [32,33].

We implemented a conductance-based thalamo-cortical circuit with realistic intrinsic dynamics, to assay both changes in cortical and thalamo-cortical population connectivity and receptor dynamics underlying observed spectral changes induced by a subanaesthetic, anti-depressant relevant dose of ketamine, as recorded with magnetoencephalography (MEG). We hypothesised that alterations in NMDA receptor activity would be identified under this manipulation and further sought to identify additional effects that might underlie Ketamine's complex dose-dependent role as a psychotomimetic and anti-depressant.

## Methods

### Sample characteristics

Details of the sample and procedures of this study have been reported previously, see Shaw et al 2015[11]. Twenty healthy (American Society of Anaesthesiologists, physical status Class 1), non-smoking, male volunteers with a BMI of 18-30 kg/m$^2$ and aged between 18 – 45 took part in the study. All subjects gave informed consent, with experimental procedures approved by the UK National Research Ethics Service in South East Wales. Subjects were screened for personal history of neurological or psychiatric disease by the Mini International Neuropsychiatric Interview[34]. Exclusion criteria further included contraindications to MEG or magnetic resonance imaging (MRI), and self-reported needle phobia.

### Visual paradigm

Subjects were presented with an annular, stationary, square-wave visual grating of spatial frequency 3 cycles per degree on a mean luminance background. Gratings were displayed 150 times, with 75 at 100% contrast and 75 at 75% contrast[35]. Grating visual angle was 8º. Subjects were instructed to focus on a small, red, continually displayed dot at the centre of the grating. To maintain attention, participants were asked to press a button with their right index finger at stimulus offset. Gratings were displayed for 1.5 to 2 s (jittered offset), with a 3 s inter-stimulus interval. Gratings were displayed on a Sanyo XP41 LCD back-projection system displaying at 1024x768 at 60 Hz.

### MEG recordings, MRI and analyses

The 275-channel MEG suite at CUBRIC (CTF MEG by MEG International Services) was operated in the supine position for comfort and to minimise head movements during sedation. A further 29 channels were recorded for noise cancellation. Fiducial (reference) coils were attached 1 cm superior to the nasion and, bilaterally, 1 cm anterior to the tragus for assessment of head position within the MEG dewar. MEG data were sampled at 1200 Hz using axial gradiometers analysed as synthetic third-order gradiometers [36,37].

All subjects underwent a structural T1-weighted scan, for co-registration to MEG, using a GE HDx 3T MR scanner with 8 channel head coil. A fast spoiled gradient echo sequence was obtained with 1 mm isotropic voxel resolution.

Pre-processing of MEG data included trial rejection by visual inspection for gross artefact using CTF DataEditor. Visual responses were localised using the synthetic aperture magnetometry (SAM) beamformer spatial filter with 4 mm isotropic resolution. A global covariance matrix (i.e. including all trials) was computed on data filtered to the visual gamma range, 30 – 80 Hz. Pseudo-t statistics were computed for baseline (-1.5 – 0 s) vs. stimulus (0 – 1.5 s). Virtual sensors were reconstructed in visual

cortex at the location of peak t-statistic. Spectra were computed using a fast Fourier transform of the virtual sensor.

Ketamine and placebo infusion protocol

All subjects underwent both a ketamine and a placebo infusion, in counterbalanced, pseudo-random order, with at least 2 weeks between sessions. The ketamine infusion consisted of 0.5mg/kg (of body mass) racemic ketamine hydrochloride in 50 ml saline. For placebo, 50 ml saline only was used. Infusions were administered by intravenous cannula in the dorsum of the left hand, with an initial bolus (~ 1 minute) of 0.25 mg/kg followed by maintenance infusion of .25 mg/kg delivered over 40 minutes. Maintenance infusion was controlled by an Asena-PK infusion pump (Alaris Medical, UK).

Modelling analysis

We implemented a thalamo-cortical model based upon Morris-Lecar[38] conductance equations, as per the model of Moran and colleagues[39–41]. The model consisted of 6 inter-connected cortical populations (pyramidal, interneuron and stellate) and 2 thalamic populations (reticular and relay), figure 1. Populations were connected in a laminar structure in accord with their anatomical position and connections though the model does not explicitly encode spatial distribution. This meant we had pyramidal and interneuron populations in layer 2/3 and layer 5, a stellate population in layer 4, and a thalamic-projection pyramidal population in layer 6. The time evolution of each population was governed by coupled differential equations describing the rate of change of membrane potential and rate of change of conductances supported by particular receptors;

$$C\frac{dV}{dt} = \sum g_k(V - V_k) + u$$
$$\dot{g}_k = \kappa_k(\varsigma_k - g_k)$$
$$k = \{AMPA, NMDA, GABA_A, GABA_B, m, h\} \tag{1}$$

Where V is the membrane potential, $g_k$ is the conductance from a particular receptor type and $g_k(V - V_k)$ represents the contribution to the membrane potential of channel k, C is the membrane capacitance, $V_k$ reversal potential of channel k and u is input current.

In the conductance equation, $\kappa_k$ is the decay rate of currents mediated by channel *k and* $\varsigma_k$ represents presynaptic input (firing rate x connectivity – see below). Conductance terms are included for 6 channels, AMPA, NMDA, $GABA_A$, $GABA_B$, m-currents and h-currents, from voltage-gated and leak potassium channels respectively. Only layer 6 thalamic-projection pyramids and thalamic relay populations possess m and h channels (see figure 1). This formulation is an extension of the NMDA-possessing model of Moran[39,41] (CMM_NMDA in the SPM DCM toolbox) and includes the same voltage switch to represent the NMDA magnesium block;

$$f_{MG}(V) = \frac{1}{1 + 0.2\exp(-\alpha_{NMDA}V)} \tag{2}$$

Reversal potentials and decay rates (table 1) were obtained from existing models[39,41] and from the literature ($GABA_B$[42], M-channel[43,44], H-channel[45]). M-channels are responsible for m-currents; non-inactivating voltage-gated potassium currents, which may be important to the intrinsic dynamics (oscillations) of the cell membrane[44]. H-channels produce hyperpolarisation activated currents, which not only have a role in the regulation of the resting membrane potential[46] but may contribute to macroscopic network oscillations[45]. The G-protein coupled $GABA_B$ receptor has also been linked to macroscale oscillations, including in the gamma range[47], possibly through its ability to re-balance the excitation-inhibition balance through interactions with NMDA receptor mediated currents[48].

| Channel | ion | Reversal (mV) | Decay rate (ms) |
|---|---|---|---|
| Potassium Leak | K | -70 | ~ |
| AMPA | Na | 60 | 4 |
| NMDA | Ca | 10 | 100 |
| GABAA | Cl | -90 | 16 |
| GABAB | ~ | -100 | 200 |
| M | K | -70 | 160 |
| H | | -30 | 100 |

Table 1. Reversal potentials and receptor decay constants for each channel in the model.

For each population in the model, the input to population *i*, is the expected firing rate from the source population *j*; the coupling of this presynaptic input to a postsynaptic response is represented by the parameter $\gamma_{(i,j)}$ which subsumes various biophysical processes such as receptor binding and transmitter reuptake.

$$\varsigma = \gamma_{i,j}\sigma(\mu_v^j - V_R, \sum j) \tag{3}$$

Here, the sigmoid function sigma represents the cumulative distribution function of the presynaptic depolarisation around a threshold potential of $V_R$ = -40 mV, which determines the proportion of cells firing[39,49].

The model was integrated numerically over a 3 s period (ensuring steady-state) at dt = 1/1200 s using an Euler method with delays as per David et al[50]. Input was a constant direct-current to thalamic relay cells. The cortex-thalamus-cortex loop took 80 ms, made up of 60 ms cortex to thalamus and 20 ms thalamus to cortex, in accordance with previous models[51,52]. The spectral response was calculated by Fourier transform of a weighted sum of the population membrane potentials (superficial pyramidal * 0.8 + spiny stellate * 0.2 + layer 5 pyramidal * 0.2 + layer 6 pyramidal * 0.2). The first 300 ms of simulation was disregarded.

The model was fitted to the MEG virtual sensor frequency spectrum between 4 and 80 Hz using the DCM Gauss-Newton optimisation routine (a Variational Laplace / Bayesian inversion routine for nonlinear models, see spm_nlsi_GN.m), which minimises a free energy term[53–55] in order to maximise the model evidence and produce a-posteriori estimates for the model parameters, which included intrinsic connectivity parameters ($\gamma$ in eq.3) and receptor time constants for AMPA, $GABA_A$, NMDA and $GABA_B$ ($\kappa$ in eq.1).

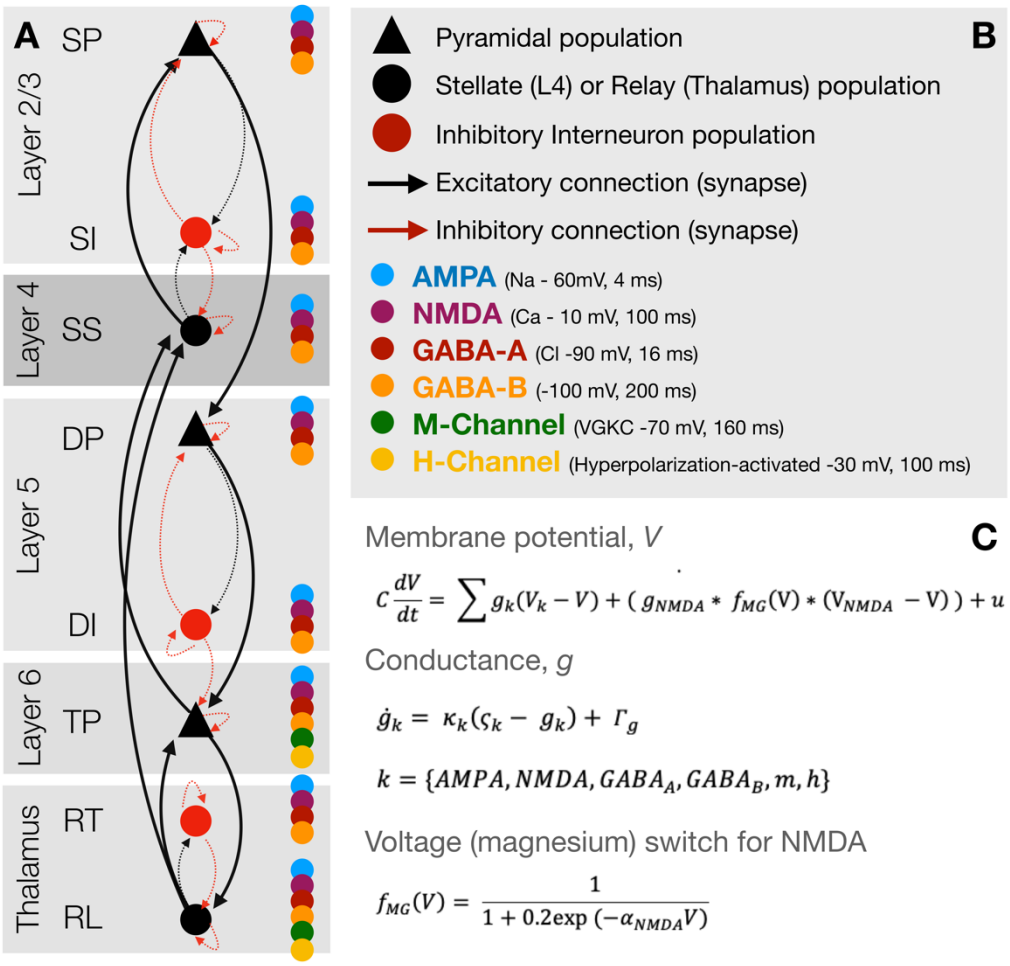


Figure 1. (A) Overview of the thalamo-cortical column architecture and connectivity. Coloured dots represent which channels are present on the population. (B) Key for the symbols in (A). (C) Summary of the conductance-based equations of motion for each population. SP = layer 2/3 (superficial) pyramidal, SI = superficial interneurons, SS = layer 4 spiny-stellates, DP = layer 5 (deep) pyramidal, DI = deep interneurons, TP = thalamic projection pyramidal (with M- and H-currents), RT = thalamic reticular and RL = thalamic relay.

<u>Study objectives</u>

In this study, we had 2 key objectives. First, to assess how well the model recapitulated the broadband spectrum of the MEG virtual sensors, and whether the model fits were adequately accurate to recapitulate the drug effects on the spectrum.

Second, given adequately fitted models, we were specifically interested in examining the effects of ketamine, as compared to placebo, on 2 sets of model parameters – as well as how these parameter effects change the output spectrum of the model. The parameter sets included (1.) the time-constants of the modelled receptors (AMPA, NMDA, GABAA and GABAB; not m- or h- channels as there were not parameterised but reflect intrinsic population dynamics) and (2.) the synaptic connectivity between populations, as reflected in figure 1(A). Between drug differences were determined by paired-t test with 5000 permutations and omnibus correction for multiple comparisons[56]. For the time-constants, this correction was for the 4 TC parameters. For the synaptic connectivity parameters, this correction was for 22 parameters (those depicted in figure 1(A), minus the 2 connections originating from reticular populations, which were fixed because they had no effect on the model output).

## Results

### Participants

Of 20 recruited subjects (mean age 25.7, SD 6.2), 1 subject withdrew prior to ketamine infusion, and an error in MEG acquisition was made for another. A further 2 datasets from the visual paradigm reported here, were rejected based on visual inspection of gross recording artifacts (reported previously[57]), resulting in 16 usable, complete (i.e. including ketamine + placebo) datasets for analysis.

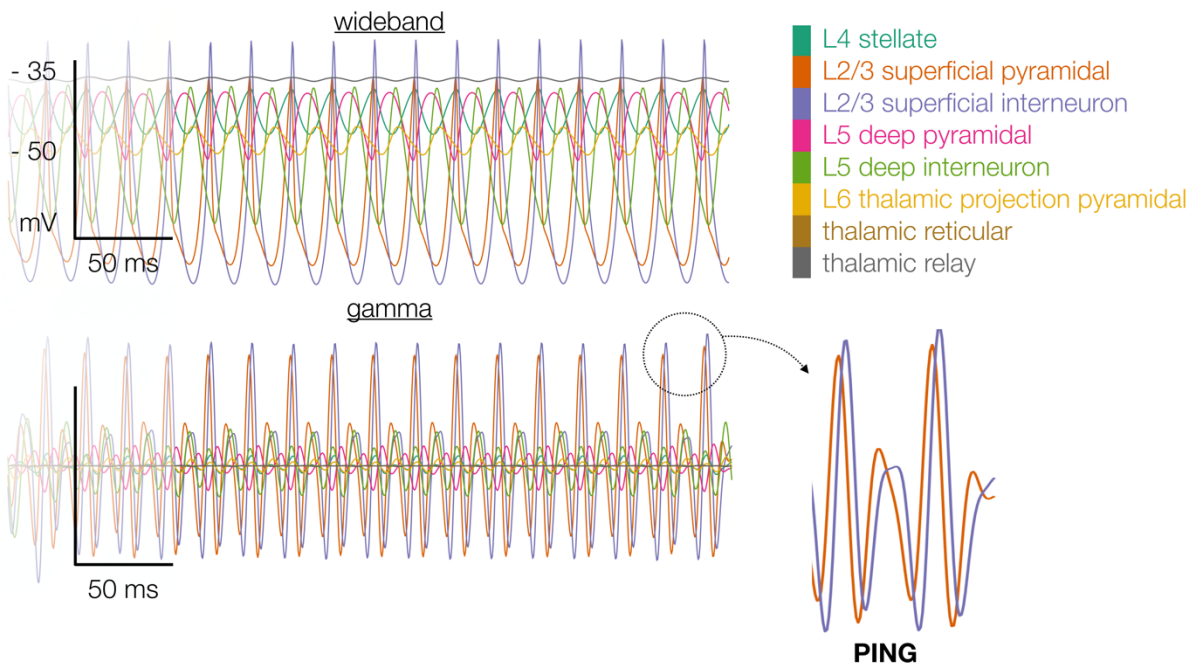


Figure 2. Example membrane potentials for a single model, showing sustained oscillatory activity at multiple frequencies. Note the strongest generators of the gamma rhythm correspond to the well characterised pyramidal-interneuron gamma (PING) network, residing in superficial layers of cortex.

### Model fits & recapitulates broadband spectral changes induced by ketamine

Although model fitting and subsequent analyses are carried out in the frequency domain, we visually confirmed the presence of sustained membrane potential oscillations (see figure 2 example) in all datasets.

Assessment of the model fits (figure 3) demonstrated good correspondence between the MEG virtual sensor spectrum, and model predicted spectrum. Quantifying this using a correlation of the amplitude at each frequency point (figure 3B) between the real and model spectrum suggested that, over the group, the model was able to recapitulate the whole spectrum, declining only at higher frequencies (> 70 Hz) and only non-significantly at 80 Hz.

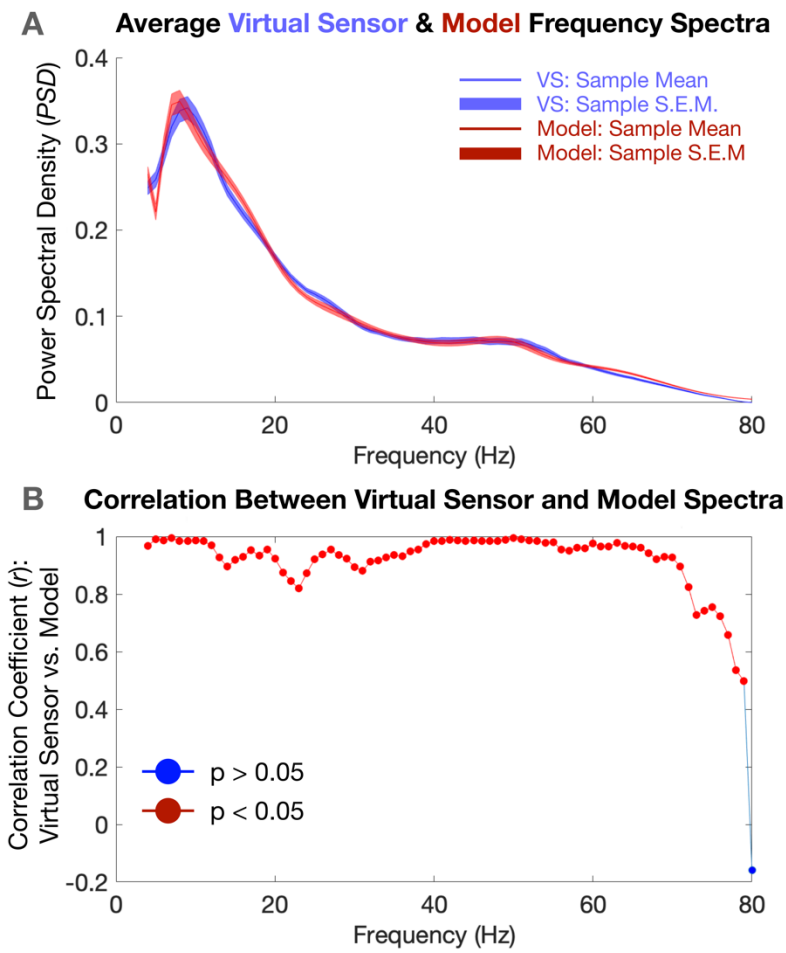


Figure 3. (A) Showing the group mean power-frequency spectrum for the MEG virtual sensor (blue) and model predictions (red). Bars represent standard error of the mean (SEM). (B) The correlation of the amplitude at each frequency step between MEG virtual sensor ('real data') and model predictions. Red dots represent p<=0.05.

We used a paired-*t* statistic with 5000 permutations and omnibus correction for multiple comparisons[56] to quantify ketamine induced changes in the spectra of both the MEG virtual sensor data, and the model predicted spectra (figure 4). In accordance with previous reports[23,24] and with previous analyses of this data[57], ketamine reduced the amplitude of lower frequencies (theta, alpha) and increased the amplitude of higher, gamma frequencies (figure 4A). Applying the same procedure to the model output revealed the same statistical pattern, demonstrating that the model fits were sufficiently accurate enough to recapitulate the drug induced spectral changes (figure 4B).

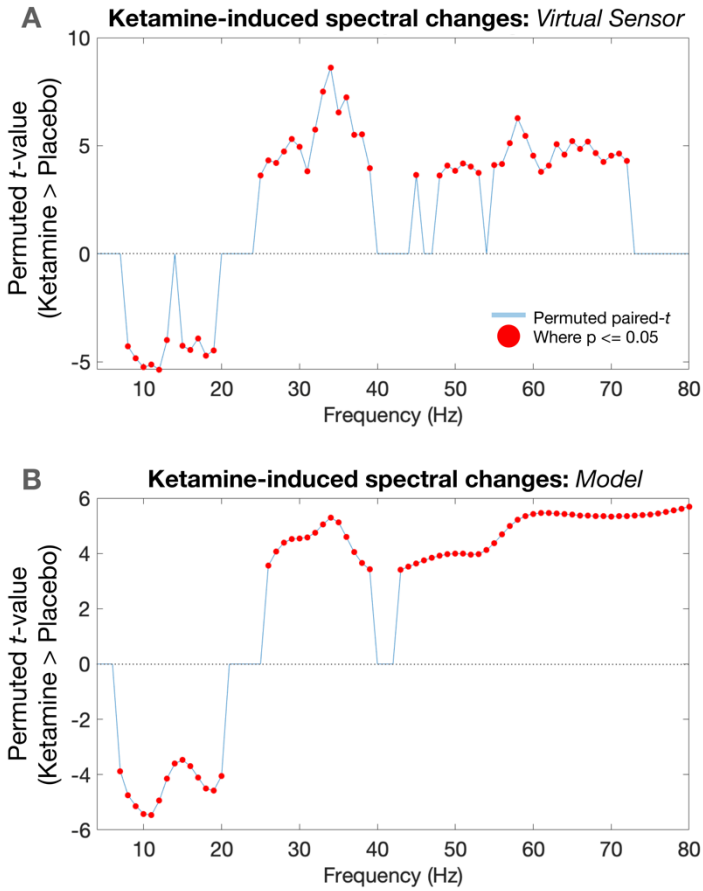


Figure 4. (A) Red dots represent significant change in amplitude at this frequency point with ketamine; the amplitudes of low frequencies are attenuated by ketamine while amplitudes of high frequencies are increased by ketamine. (B) Showing the same drug-effects on the model spectrum.

<u>Model parameters analysis: receptor decay constants and intrinsic coupling</u>

The receptor decay time constant (TC, $\kappa$ in equation 1) of NMDA channels was shorter (faster decay) with ketamine compared to placebo (t = -2.64, p = 0.046 corrected), figure 5(C). The TC of GABAB was longer (slower decay) with ketamine compared to placebo (t = 2.99, p = 0.020 corrected). There was no difference in the TCs of either AMPA or $GABA_A$ channels.

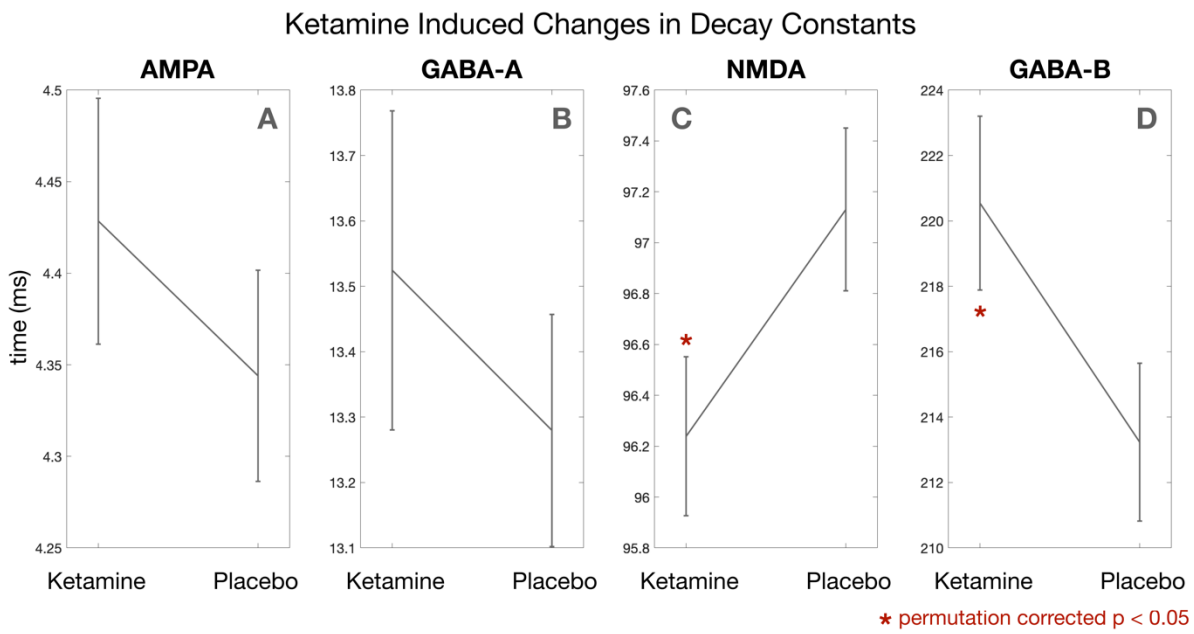


Figure 5. Ketamine and placebo group means and standard deviations of the posterior receptor decay constants for AMPA (A), $GABA_A$ (B), NMDA (C) and $GABA_B$ (D). Ketamine significantly increased the rate of decay of NMDA currents (corrected p = 0.046) and decreased the rate of decay of $GABA_B$ currents (corrected p = 0.02).

Three connectivity parameters were different between ketamine and placebo conditions; inhibitory SP→SP self-modulation decreased with ketamine (t = -3.01, p = 0.020), inhibitory SI→SI self-modulation increased with ketamine (t = 2.75, p = 0.024) and the cortico-thalamic projection from layer 6 pyramids into thalamic relay populations was increased with ketamine (t = 3.13, p = 0.012).

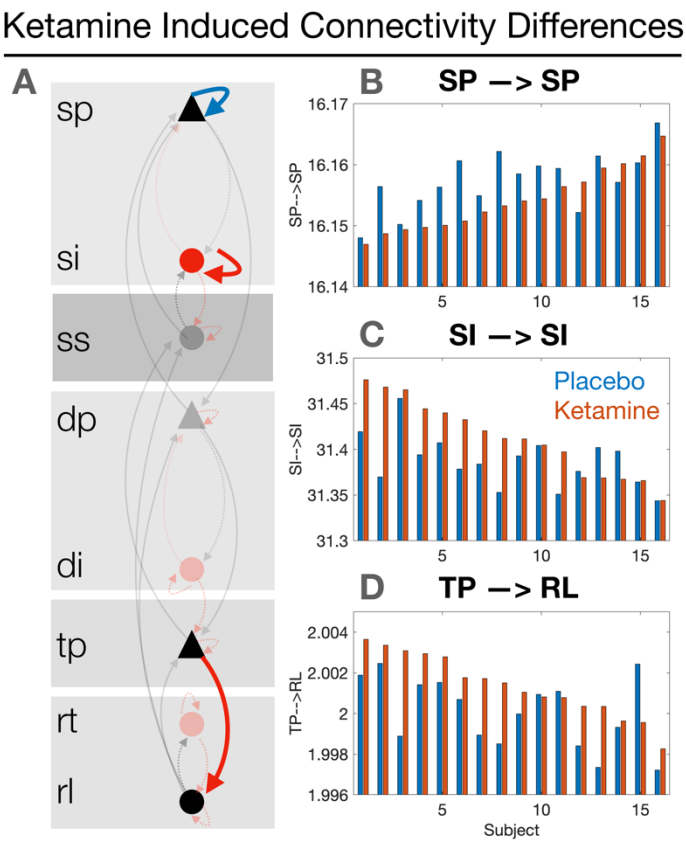


Figure 6. Ketamine induced changes in connectivity between populations (cf. synaptic connectivity), shown topographically (A). (A) Showing the 3 corrected-significant parameters (red = increased by ketamine). (B), (C) and (D) show the subject specific parameters for SP→SP, SI→SI and TP→RL.

<u>*In silico* rectification of ketamine-induced receptor changes and corresponding spectral changes</u>

For each of the 5 parameter differences induced by ketamine (alterations of NMDA and $GABA_B$ TCs, and connections SP→SP, SI→SI and TP→RL), we performed *in-silico* 'rectifications' of these parameters by re-running the fitted ketamine models with each of the parameters shifted to the corresponding value from that subject's placebo model.

Quantifying the change in spectral features for the rectified NMDA TC, expressed as percentage-change from baseline ketamine model, demonstrated an increase in the amplitude of alpha, centred on 10 Hz (mean +1.6%) and small reductions in gamma at around 50 Hz (mean -0.2%) (figure 7A). As the baseline effect of ketamine, relative to placebo, was to reduce lower frequency amplitudes while boosting higher frequencies, the shift induced here moves the spectrum towards the placebo state. Performing the same quantification for the rectified $GABA_B$ TC revealed the same pattern of changes, but with small effect (mean alpha amplitude +0.25% at 10 Hz, mean gamma -0.02% peaking at 48 Hz, see figure 7B).

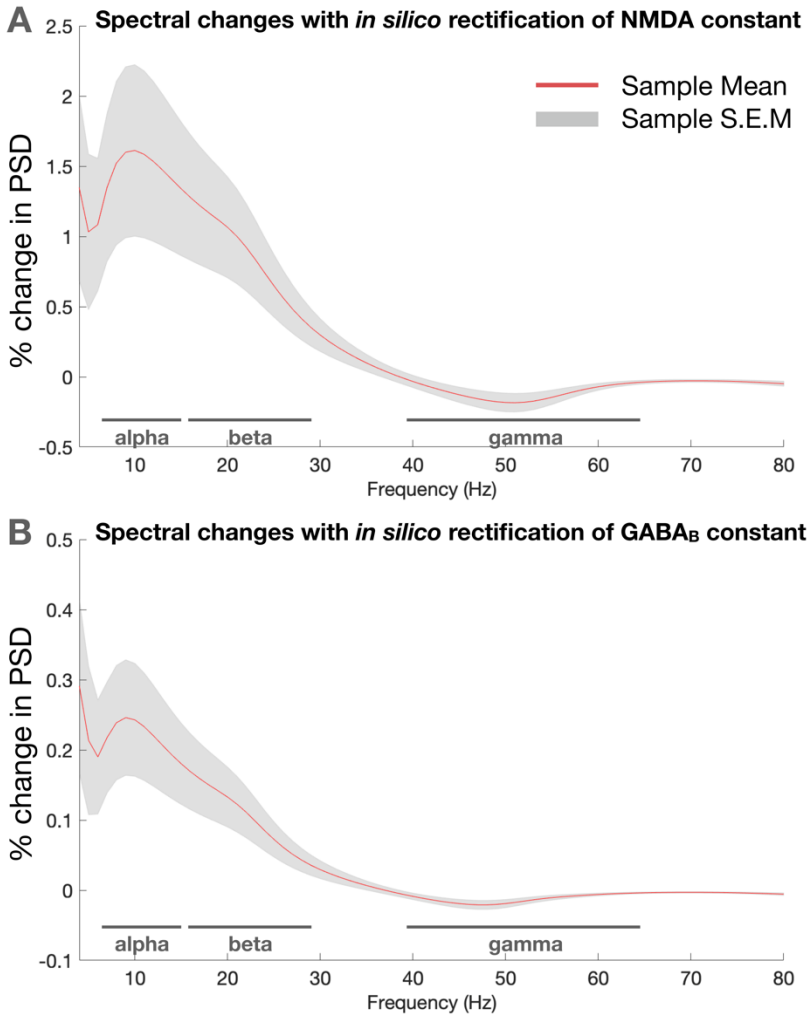


Figure 7. Changes to the spectrum from the baseline ketamine model to the (A) NMDA-channel 'rectified' model, shown as percent-change at each frequency point. Changing this parameter shows clear increases in the PSD in alpha and beta and modest reductions in PSD at gamma frequencies, mirroring the original drug effects, where ketamine decreased the PSD at lower frequencies and increased it at gamma frequencies. (B) The GABA$_B$-channel 'rectified' model, again showing percentage-change from baseline ketamine model when returning this parameter to the placebo state. Effects are similar to the NMDA channel but with smaller %-change effects.

Quantifying the change in spectral features induced by rectifying each of the 3 connectivity parameters (c.f. sensitivity analysis) revealed similar effects for SP→SP, SI→SI and TP→RL (figure 8). This included increasing the amplitude of low frequencies, centred on a 10 Hz peak (mean increases of +0.12%, +1.85% and +0.77% for SP→SP, SI→SI and TP→RL, respectively). Moreover, all three parameters induced decreases in the gamma band, with peaks at 45 Hz (SP→SP, -0.02%), 51 Hz (TP→RL, -0.07%) and 55 Hz (SI→SI -0.12%).

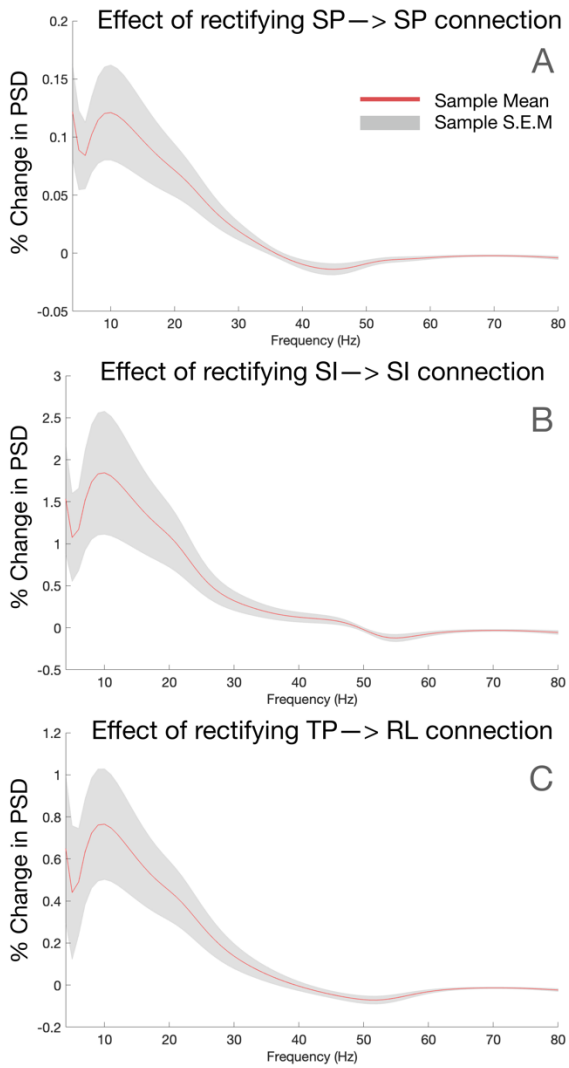


Figure 8. Changes to the spectrum from the baseline ketamine model, induced by 'rectifying' each of the parameters to its placebo-model state for (A) layer 2/3 SP→SP, (B) SI→SI and (C) TP→RL (cortico-thalamic projection). All parameters show a general effect of increasing the PSD at lower frequencies. (A) slightly reduced the PSD at 45 Hz, (C) at 51 Hz and (B) at 55 Hz.

## Discussion

### Model sensitivity

In this study, we have demonstrated that a simplified thalamo-cortical model, implemented with DCM, is able to recapitulate the spectral changes induced by subanaesthetic ketamine administration during a visual grating task. Comparing the models fitted to ketamine and placebo, we identify 5 key parameters that were changed by ketamine; namely, the receptor decay constants of NMDA (shortened) and $GABA_B$ (lengthened) channels, the inhibitory self-modulation of superficial pyramidal (decreased) and inhibitory interneurons (increased) and the cortico-thalamic projection from layer 6 into thalamic relay populations (increased).

We assessed the goodness-of-fit of the model spectra using correlations over all datasets of the amplitude at each frequency step, comparing the model and 'real', MEG virtual sensor spectra. As evidenced in figure 3, the model accurately summarized the features of the real spectrum, with significant correlations through much of the frequency spectrum, declining only at higher frequencies (> 70 Hz) and only non-significantly at 80 Hz.

Before making any between-drug parameter inference, it was important to assess whether the model had summarized the data well enough to be sensitive to the drug induced changes in the spectrum. As shown in figure 4, the spectral difference in amplitude observed in the empirical MEG data (figure 4A), which included significant reductions in alpha amplitude and increases in gamma amplitude, were also evident at the same frequencies in the model output (figure 4B).

### Ketamine parameter effects

- *NMDA channel decay time constant*

While its pharmacological profile is known to be complex[58], the key mechanism of action of ketamine is thought to be as an uncompetitive antagonist of NMDA receptors, binding at the dizocilpine (MK-801) site[58,59]. Predicting the effect that antagonising the channel might have on the (modelled) channel decay constant is difficult. However, a study of the effects of both ketamine and MK-801 (also an NMDA antagonist, binding at the same site) on NMDA receptor mediated currents in hippocampal cultured neurons, demonstrated that administration of ketamine or MK-801 significantly increased the rate at which excitatory postsynaptic currents decayed[60]. This is entirely in keeping with our result, where compared to placebo, the decay constant of NMDA channels was significantly shorter with ketamine.

- *$GABA_B$ channel decay time constant*

Within the context of our model, ketamine significantly lengthened the decay constant of $GABA_B$ channels. It is unlikely that ketamine directly binds to $GABA_B$ receptors, so this change likely reflects a

downstream effect of NMDA receptor antagonism[48,61]. In NMDA-deficient mice, it has been demonstrated that agonism of $GABA_B$ receptors improves excitation-inhibition balance and restores high frequency oscillatory activity[48]. Other studies have also suggested a role for $GABA_B$ receptors in shaping high frequency oscillations[47,62], while recent efforts to understand the antidepressant effects of ketamine have suggested a possible role for $GABA_B$ receptors[61,63].

- *Disinhibition within SP populations (SP→SP)*

Ketamine was found to decrease the strength of the inhibitory self-modulation connection on superficial pyramidal populations (akin to a small, local inhibitory pool), compared to placebo. This parameter corresponds not only to a crucial synaptic determinant of gamma oscillatory activity[1,64–69], but is also the key parameter in our model corresponding to the phenomenon of disinhibition[70]. Disinhibition by NMDA antagonism[71], a prominent theory of schizophrenia[72–74], describes a mechanism by which hypofunction of NMDA receptors results in reduced local inhibition, which in turn results in disinhibition of superficial pyramidal populations. This disinhibited, aberrant state disrupts local signalling, processing and alters gamma oscillations[70,72,75]. It has been proposed as a candidate mechanism by which ketamine disrupts gamma[71], a theory which our result could support.

- *Increased inhibition within SI populations (SI→SI)*

Ketamine was found to increase the inhibitory self-modulation of superficial interneuron populations, compared to placebo. Initially, this result seems to contrast the theory of disinhibition outlined above, because the activity of inhibitory interneurons should be decreased[70]. This contrast may reflect the simplistic parameterisation of cortical models like ours, where every population has its own inhibitory self-modulation parameter as well as their being explicit inhibitory interneuron populations. Under this framework, increased inhibitory self-modulation of inhibitory interneurons (SI→SI) is an unrelated process to the inhibitory self-modulation of superficial pyramidal populations (SP→SP).

- *Increased cortico-thalamic output connectivity (TP→RL)*

Ketamine increased the strength of the excitatory cortico-thalamic projection from the layer 6 pyramidal population into thalamic relay population, compared to placebo. Ketamine mediated increases in cortico-thalamic connectivity have been reported in resting state functional magnetic resonance imaging (fMRI) studies[76], although this study focussed on somatosensory and temporal cortical projections[76], rather than visual.

In rat, administration of ketamine was found to enhance the visual cortex layer 6 projection to thalamus[77], mimicking exactly the alteration found in our model. They also demonstrated that this connection predicted the amplitude of thalamic gamma oscillations[77], however qualitative assessment of the output of our fitted models did not reveal oscillations in the gamma range in the membrane potential of thalamic populations.

Parameter rectification and spectral effects

For each of the previously described 5 parameter changes, we quantified the effect that restoring that parameter (to its value from the placebo model) had on the output spectrum. This *in-silico* 'reverse lesioning' allowed us to understand the effect that each of the ketamine-altered parameters had on the output of the model. Or, which parameter changes might underlie which spectral changes induced by ketamine.

Quantifying the parameter changes as percent-change from the baseline fitted ketamine model c.f. a sensitivity analysis, all five parameters demonstrated similar effects of increasing the amplitude of low frequency oscillations (which had been reduced by ketamine) and reducing the amplitude of high frequency, gamma oscillations (which had been increased by ketamine). Effects of the NMDA and $GABA_B$ TCs were to increase the 10 Hz alpha by +1.6% and +0.25%, respectively. The NMDA TC reduced gamma with peak effect at 50 Hz, by -0.2%, while the GABAB TC reduced gamma with a peak effect at 48 Hz, by 0.02%. The 3 connectivity parameters all also increased alpha at 10 Hz, but with varying peak frequency effects (SP→SP 45 Hz -0.02%, TP→RL 51 Hz -0.07% and SI→SI 55 Hz, -0.12%).

Study limitations and future work

Given the sensitivity of model parameters to manipulation by ketamine, it would be interesting to know whether any of the observed effect are dose-dependent, particularly since ketamine has seen a resurgence in popularity due to its antidepressant effects. In the present study, we used a fixed 0.5mg/kg dose, however there have been no neuroimaging-based studies of ketamine at varying levels, which would permit discovery of dose-dependent effects.

This study explored the effects of ketamine in healthy, young participants. However, the same modelling framework could be applied to clinical trial data, where ketamine is currently under investigation as a treatment option for a variety of psychiatric (mood) disorders. In this context, the sensitivity of model parameters could serve as sensitive and specific biomarkers – both of illness and of treatment response.

In this study, we have demonstrated that a thalamo-cortical circuit, fitted to empirical pharmaco-MEG data with DCM, is accurate enough to recapitulate spectral changes induced by ketamine; and sensitive to local receptor and synaptic connectivity dynamics. We have shown that both superficial layer disinhibition and cortico-thalamic afferents play a role in shaping the oscillatory responses of ketamine, which should be considered in future studies linking gamma and disinhibition.

## Acknowledgements

This work was supported by CUBRIC and the School of Psychology at Cardiff University as well as the UK MEG MRC Partnership Grant (MRC/EPSRC, MR/K005464/1) .
ADS is supported by a Wellcome Strategic Award (104943/Z/14/Z).

## References

1. Buzsáki G, Wang X-J. Mechanisms of Gamma Oscillations. *Annu Rev Neurosci*. 2012;35(1):203-225. http://www.annualreviews.org/doi/abs/10.1146/annurev-neuro-062111-150444.
2. Brunel N, Wang X-J. What determines the frequency of fast network oscillations with irregular neural discharges? I. Synaptic dynamics and excitation-inhibition balance. *J Neurophysiol*. 2003;90(1):415-430. doi:10.1152/jn.01095.2002
3. Ward LM. Synchronous neural oscillations and cognitive processes. *Trends Cogn Sci*. 2003;7(12):553-559. http://eutils.ncbi.nlm.nih.gov/entrez/eutils/elink.fcgi?dbfrom=pubmed&id=14643372&retmode=ref&cmd=prlinks.
4. Özerdem A, Güntekin B, Tunca Z, Başar E. Brain oscillatory responses in patients with bipolar disorder manic episode before and after valproate treatment. *Brain Res*. 2008;1235:98-108. doi:10.1016/j.brainres.2008.06.101
5. Herrmann CS, Demiralp T. Human EEG gamma oscillations in neuropsychiatric disorders. *Clin Neurophysiol*. 2005;116(12):2719-2733. doi:10.1016/j.clinph.2005.07.007
6. Hansenne M. Event-related brain potentials in psychopathology: Clinical and cognitive perspectives. *Psychol Belg*. 2006;46(1-2):5-36.
7. Perry G, Brindley LM, Muthukumaraswamy SD, Singh KD, Hamandi K. Evidence for increased visual gamma responses in photosensitive epilepsy. *Epilepsy Res*. 2014;108(6):1076-1086. http://eutils.ncbi.nlm.nih.gov/entrez/eutils/elink.fcgi?dbfrom=pubmed&id=24893831&retmode=ref&cmd=prlinks.
8. Nishida K, Yoshimura M, Isotani T, et al. Differences in quantitative EEG between frontotemporal dementia and Alzheimer's disease as revealed by LORETA. *Clin Neurophysiol*. 2011;122(9):1718-1725. doi:10.1016/j.clinph.2011.02.011
9. Tan HRM, Lana L, Uhlhaas PJ. High-frequency neural oscillations and visual processing deficits in schizophrenia. *Front Psychol*. 2013;4(OCT):1-19. doi:10.3389/fpsyg.2013.00621
10. Muthukumaraswamy SD. The use of magnetoencephalography in the study of psychopharmacology (pharmaco-MEG). *J Psychopharmacol*. 2014;(June). doi:10.1177/0269881114536790
11. Shaw AD, Saxena N, E Jackson L, Hall JE, Singh KD, Muthukumaraswamy SD. Ketamine amplifies induced gamma frequency oscillations in the human cerebral cortex. *Eur Neuropsychopharmacol*. 2015;25(8):1136-1146. doi:10.1016/j.euroneuro.2015.04.012
12. Muthukumaraswamy SD, Routley B, Droog W, Singh KD, Hamandi K. The effects of AMPA

blockade on the spectral profile of human early visual cortex recordings studied with non-invasive MEG. *Cortex*. 2016;81:266-275. doi:10.1016/j.cortex.2016.03.004

13. Saxena N, Muthukumaraswamy SD, Diukova A, Singh K, Hall J, Wise R. Enhanced Stimulus-Induced Gamma Activity in Humans during Propofol-Induced Sedation. *PLoS One*. 2013;8(3):e57685. http://www.plosone.org/article/info%3Adoi%2F10.1371%2Fjournal.pone.0057685.
14. Campbell AE, Sumner P, Singh KD, Muthukumaraswamy SD. Acute Effects of Alcohol on Stimulus-Induced Gamma Oscillations in Human Primary Visual and Motor Cortices. 2014:1-10. http://dx.doi.org/10.1038/npp.2014.58.
15. Magazzini L, Muthukumaraswamy SD, Campbell AE, et al. Significant reductions in human visual gamma frequency by the gaba reuptake inhibitor tiagabine revealed by robust peak frequency estimation. *Hum Brain Mapp*. 2016;3896:3882-3896. doi:10.1002/hbm.23283
16. Bastos AM, Briggs F, Alitto HJ, Mangun GR, Usrey WM. Simultaneous Recordings from the Primary Visual Cortex and Lateral Geniculate Nucleus Reveal Rhythmic Interactions and a Cortical Source for Gamma-Band Oscillations. *J Neurosci*. 2014;34(22):7639-7644. http://www.jneurosci.org/cgi/doi/10.1523/JNEUROSCI.4216-13.2014.
17. Hall SD, Holliday IE, Hillebrand A, et al. The missing link: analogous human and primate cortical gamma oscillations. *Neuroimage*. 2005;26(1):13-17. http://eutils.ncbi.nlm.nih.gov/entrez/eutils/elink.fcgi?dbfrom=pubmed&id=15862200&retmode=ref&cmd=prlinks.
18. Perry G, Hamandi K, Brindley LM, Muthukumaraswamy SD, Singh KD. NeuroImage The properties of induced gamma oscillations in human visual cortex show individual variability in their dependence on stimulus size. *Neuroimage*. 2013;68:83–92. doi:10.1016/j.neuroimage.2012.11.043
19. Gray CM, Singer W. Stimulus-specific neuronal oscillations in orientation columns of cat visual cortex. *Proc Natl Acad Sci U S A*. 1989;86(5):1698-1702. doi:10.1073/pnas.86.5.1698
20. Clayton MS, Yeung N, Cohen Kadosh R. The many characters of visual alpha oscillations. *Eur J Neurosci*. 2017;(September):1-11. doi:10.1111/ejn.13747
21. Xing D, Yeh C-I, Burns S, Shapley RM. Laminar analysis of visually evoked activity in the primary visual cortex. *Proc Natl Acad Sci*. 2012;109(34):13871-13876. http://eutils.ncbi.nlm.nih.gov/entrez/eutils/elink.fcgi?dbfrom=pubmed&id=22872866&retmode=ref&cmd=prlinks.
22. Schmiedt JT, Maier A, Fries P, Saunders RC, Leopold DA, Schmid MC. Beta Oscillation Dynamics in Extrastriate Cortex after Removal of Primary Visual Cortex. *J Neurosci*. 2014;34(35):11857-11864. doi:10.1523/JNEUROSCI.0509-14.2014
23. Hong LE, Summerfelt A, Buchanan RW, et al. Gamma and delta neural oscillations and association with clinical symptoms under subanesthetic ketamine. *Neuropsychopharmacology*. 2010;35(3):632-640. doi:10.1038/npp.2009.168
24. Lazarewicz MT, Ehrlichman RS, Maxwell CR, Gandal MJ, Finkel LH, Siegel SJ. Ketamine

modulates theta and gamma oscillations. *J Cogn Neurosci*. 2010;22(7):1452-1464. doi:10.1162/jocn.2009.21305

25. Maier A, Adams GK, Aura C, Leopold DA. Distinct Superficial and Deep Laminar Domains of Activity in the Visual Cortex during Rest and Stimulation. *Front Syst Neurosci*. 2010;4. http://journal.frontiersin.org/Journal/10.3389/fnsys.2010.00031/full.
26. Halgren M, Devinsky O, Doyle WK, et al. The Generation and Propagation of the Human Alpha Rhythm. *bioRxiv*. 2017:202564. doi:10.1101/202564
27. Lorincz ML, Kékesi KA, Juhász G, Crunelli V, Hughes SW. Temporal Framing of Thalamic Relay-Mode Firing by Phasic Inhibition during the Alpha Rhythm. *Neuron*. 2009;63(5):683-696. doi:10.1016/j.neuron.2009.08.012
28. Friston KJ, Harrison L, Penny W. Dynamic causal modelling. *Neuroimage*. 2003. http://www.sciencedirect.com/science/article/pii/S1053811903002027.
29. Kiebel SJ, Garrido MI, Moran RJ, Friston KJ. Dynamic causal modelling for EEG and MEG. *Cogn Neurodyn*. 2008;2(2):121-136. doi:10.1007/s11571-008-9038-0
30. Moran RJ, Kiebel SJ, Stephan KE, Reilly RB, Daunizeau J, Friston KJ. A neural mass model of spectral responses in electrophysiology. *Neuroimage*. 2007;37(3):706-720. http://eutils.ncbi.nlm.nih.gov/entrez/eutils/elink.fcgi?dbfrom=pubmed&id=17632015&retmode=ref&cmd=prlinks.
31. Moran RJ, Stephan KE, Dolan RJ, Friston KJ. Consistent spectral predictors for dynamic causal models of steady-state responses. *Neuroimage*. 2011;55(4):1694-1708. http://linkinghub.elsevier.com/retrieve/pii/S1053811911000309.
32. Phillips HN, Blenkmann A, Hughes LE, Kochen S, Bekinschtein TA, Rowe JB. ScienceDirect Convergent evidence for hierarchical prediction networks from human electrocorticography and magnetoencephalography. *CORTEX*. 2016;82:192-205. doi:10.1016/j.cortex.2016.05.001
33. Moran RJ, Jung F, Kumagai T, et al. Dynamic causal models and physiological inference: a validation study using isoflurane anaesthesia in rodents. *PLoS One*. 2011;6(8):e22790. http://eutils.ncbi.nlm.nih.gov/entrez/eutils/elink.fcgi?dbfrom=pubmed&id=21829652&retmode=ref&cmd=prlinks.
34. Sheehan D V., Lecrubier Y, Sheehan KH, et al. The Mini-International Neuropsychiatric Interview (M.I.N.I.): The development and validation of a structured diagnostic psychiatric interview for DSM-IV and ICD-10. In: *Journal of Clinical Psychiatry*. ; 1998. doi:10.1016/S0924-9338(99)80239-9
35. Muthukumaraswamy SD, Singh KD. Visual gamma oscillations: the effects of stimulus type, visual field coverage and stimulus motion on MEG and EEG recordings. *Neuroimage*. 2013;69:223-230. http://eutils.ncbi.nlm.nih.gov/entrez/eutils/elink.fcgi?dbfrom=pubmed&id=23274186&retmode=ref&cmd=prlinks.
36. Vrba J. Signal Processing in Magnetoencephalography. *Methods*. 2001;25(2):249-271. http://linkinghub.elsevier.com/retrieve/pii/S1046202301912381.

37. Robinson S, Vrba J. *Recent Advances in Biomagnetism. Sendai: Tohoku University Press.*; 1999.
38. Morris C, Lecar H. Voltage oscillations in the barnacle giant muscle fiber. *Biophys J*. 1981;35(1):193-213. doi:10.1016/S0006-3495(81)84782-0
39. Moran RJ, Symmonds M, Stephan KE, Friston KJ, Dolan RJ. An in vivo assay of synaptic function mediating human cognition. *Curr Biol*. 2011;21(15):1320-1325. doi:10.1016/j.cub.2011.06.053
40. Muthukumaraswamy SD, Shaw AD, Jackson LE, Hall J, Moran R, Saxena N. Evidence that Subanesthetic Doses of Ketamine Cause Sustained Disruptions of NMDA and AMPA-Mediated Frontoparietal Connectivity in Humans. *J Neurosci*. 2015;35(33):11694-11706. doi:10.1523/JNEUROSCI.0903-15.2015
41. Gilbert JR, Symmonds M, Hanna MG, Dolan RJ, Friston KJ, Moran RJ. Profiling neuronal ion channelopathies with non-invasive brain imaging and dynamic causal models: Case studies of single gene mutations. *Neuroimage*. 2016;124:43-53. doi:10.1016/j.neuroimage.2015.08.057
42. Gerstner W, Kistler WM, Naud R, Paninski L. *Neuronal Dynamics: From Single Neurons to Networks and Models of Cognition.*; 2014. doi:10.1017/CBO9781107447615
43. Brown DA, Adams PR. Muscarinic suppression of a novel voltage-sensitive K+ current in a vertebrate neurone. *Nature*. 1980;283(February):673-676.
44. Bordas C, Kovacs A, Pal B. The M-current contributes to high threshold membrane potential oscillations in a cell type-specific way in the pedunculopontine nucleus of mice. 2015;9(April):1-12. doi:10.3389/fncel.2015.00121
45. Gonzalez OJA, Mansvelder HD, Pelt J Van, Ooyen A Van. H-Channels Affect Frequency , Power and Amplitude Fluctuations of Neuronal Network Oscillations. 2015;9(November):1-14. doi:10.3389/fncom.2015.00141
46. Santoro B, Z BT. The multiple personalities of h-channels. *Trends Neurosci*. 2003;26(10):550-554.
47. Brown JT, Davies CH, Randall AD. Synaptic activation of GABAB receptors regulates neuronal network activity and entrainment. *Eur J Neurosci*. 2007;25(10):2982-2990. doi:10.1111/j.1460-9568.2007.05544.x
48. Gandal MJ, Sisti J, Klook K, et al. GABAB-mediated rescue of altered excitatory–inhibitory balance, gamma synchrony and behavioral deficits following constitutive NMDAR-hypofunction. *Transl Psychiatry*. 2012;2(7):e142. doi:10.1038/tp.2012.69
49. Marreiros AC, Kiebel SJ, Daunizeau J, Harrison LM, Friston KJ. NeuroImage Population dynamics under the Laplace assumption ☆. *Neuroimage*. 2009;44(3):701-714. doi:10.1016/j.neuroimage.2008.10.008
50. David O, Kiebel S, Harrison L, Mattout J, Kilner J, Friston K. Dynamic causal modeling of evoked responses in EEG and MEG. *Neuroimage*. 2006;30(4):1255-1272. doi:doi: 10.1016/j.neuroimage.2005.10.045

51. Hashemi M, Hutt A, Hight D, Sleigh J. Anesthetic action on the transmission delay between cortex and thalamus explains the beta-buzz observed under propofol anesthesia. 2017:1-29.
52. Roberts JA, Robinson PA. Modeling absence seizure dynamics : Implications for basic mechanisms and measurement of thalamocortical and corticothalamic latencies. 2008;253:189-201. doi:10.1016/j.jtbi.2008.03.005
53. Friston K, Kilner J, Harrison L. A free energy principle for the brain. *J Physiol*. 2006. http://www.sciencedirect.com/science/article/pii/S092842570600060X.
54. Penny WD. Comparing dynamic causal models using AIC, BIC and free energy. *Neuroimage*. 2012;59(1):319-330. doi:10.1016/j.neuroimage.2011.07.039
55. Friston K, Mattout J, Trujillo-Barreto N, Ashburner J, Penny W. Variational free energy and the Laplace approximation. *Neuroimage*. 2007;34(1):220-234. doi:10.1016/j.neuroimage.2006.08.035
56. Nichols TE, Holmes AP. Nonparametric Permutation Tests for {PET} functional Neuroimaging Experiments: A Primer with examples. *Hum Brain Mapp*. 2001;15(1):1-25. doi:10.1002/hbm.1058
57. Shaw AD, Saxena N, E Jackson L, Hall JE, Singh KD, Muthukumaraswamy SD. Ketamine amplifies induced gamma frequency oscillations in the human cerebral cortex. *Eur Neuropsychopharmacol*. 2015;25(8):1136-1146. doi:10.1016/j.euroneuro.2015.04.012
58. Zorumski CF, Izumi Y, Mennerick XS. Dual Perspectives Companion Paper : The Role of GluN2C-Containing NMDA Receptors in Ketamine ' s Psychotogenic Ketamine : NMDA Receptors and Beyond. 2016;36(44):11158-11164. doi:10.1523/JNEUROSCI.1547-16.2016
59. Johnson JW, Kotermanski SE. Mechanism of action of memantine. doi:10.1016/j.coph.2005.09.007
60. Tovar KR, Westbrook GL. Mobile NMDA Receptors at Hippocampal Synapses. 2002;34:255-264.
61. Zanos P, Gould TD. Mechanisms of ketamine action as an antidepressant. *Nat Publ Gr*. 2018;23(4):801-811. doi:10.1038/mp.2017.255
62. Craig MT, McBain CJ. The emerging role of GABAB receptors as regulators of network dynamics: fast actions from a 'slow' receptor? *Curr Opin Neurobiol*. 2014. doi:10.1016/j.conb.2013.10.002
63. Frankowska M, Filip M, Przegaliński E. Effects of GABA B receptor ligands in animal tests of depression and anxiety. 2007.
64. Sohal VS. Insights into cortical oscillations arising from optogenetic studies. *Biol Psychiatry*. 2012;71(12):1039-1045. doi:10.1016/j.biopsych.2012.01.024
65. Traub RD, Whittington M a, Colling SB, Buzsáki G, Jefferys JG. Analysis of gamma rhythms in the rat hippocampus in vitro and in vivo. *J Physiol*. 1996;493 ( Pt 2:471-484.
66. Traub RD, Spruston N, Soltesz I, Konnerth A, Whittington MA, Jefferys GR. Gamma-frequency oscillations: a neuronal population phenomenon, regulated by synaptic and intrinsic cellular processes, and inducing synaptic plasticity. *Prog Neurobiol*. 1998;55(6):563-575.

http://eutils.ncbi.nlm.nih.gov/entrez/eutils/elink.fcgi?dbfrom=pubmed&id=9670218&retmode=ref&cmd=prlinks.

67. Bartos M, Vida I, Jonas P. Synaptic mechanisms of synchronized gamma oscillations in inhibitory interneuron networks. *Nat Rev Neurosci*. 2007;8(1):45-56. doi:10.1038/nrn2044
68. Whittington MA, Traub RD, Kopell N, Ermentrout B, Buhl EH. Inhibition-based rhythms: experimental and mathematical observations on network dynamics. *Int J Psychophysiol*. 2000;38(3):315-336. http://www.sciencedirect.com/science/article/pii/S0167876000001732.
69. Shaw AD, Moran RJ, Muthukumaraswamy SD, et al. Neurophysiologically-informed markers of individual variability and pharmacological manipulation of human cortical gamma. *Neuroimage*. 2017;161(December 2016):19-31. doi:10.1016/j.neuroimage.2017.08.034
70. Homayoun H, Moghaddam B. NMDA receptor hypofunction produces opposite effects on prefrontal cortex interneurons and pyramidal neurons. *J Neurosci*. 2007;27(43):11496-11500. doi:10.1523/JNEUROSCI.2213-07.2007
71. Seamans J. Losing inhibition with ketamine. *Nature chemical biology*. file:///Users/alexandershaw/Library/Application Support/Papers2/Articles/2008/Seamans/Nat. Chem. Biol. 2008 Seamans-2.pdf. Published 2008.
72. Spencer K. The functional consequences of cortical circuit abnormalities on gamma oscillations in schizophrenia: insights from computational modeling. *Front Hum Neurosci*. 2009;3. http://www.ncbi.nlm.nih.gov/pmc/articles/PMC2769552/.
73. Frohlich J, Van Horn JD. Reviewing the ketamine model for schizophrenia. *J Psychopharmacol*. 2014;28(4):287-302. doi:10.1177/0269881113512909
74. Friston K, Brown HR, Siemerkus J, Stephan KE. The dysconnection hypothesis (2016). *Schizophr Res*. 2016;176(2-3):83-94. doi:10.1016/j.schres.2016.07.014
75. Moghaddam B, Javitt D. From revolution to evolution: The glutamate hypothesis of schizophrenia and its implication for treatment. *Neuropsychopharmacology*. 2012;37(1):4-15. doi:10.1038/npp.2011.181
76. Höflich A, Hahn A, Küblböck M, et al. Ketamine-Induced Modulation of the Thalamo- Cortical Network in Healthy Volunteers As a Model for Schizophrenia. 2015:1-11. doi:10.1093/ijnp/pyv040
77. Anderson PM, Jones NC, Brien TJO, Pinault D. The N -Methyl □ -Aspartate Glutamate Receptor Antagonist Ketamine Disrupts the Functional State of the Corticothalamic Pathway. 2017;(June 2016):3172-3185. doi:10.1093/cercor/bhw168